applied sciences

MDPI

Article

Security-Constrained Day-Ahead Operational Planning for Flexible Hybrid AC/DC Distribution Networks

Ahmad Asrul Ibrahim [1,*], Behzad Kazemtabrizi [2] and Javier Renedo [3]

[1] Center for Integrated Systems Engineering and Advanced Technologies, Universiti Kebangsaan Malaysia, 43600 Bangi, Malaysia
[2] Department of Engineering, Durham University, Durham DH1 3LE, UK; behzad.kazemtabrizi@durham.ac.uk
[3] Instituto de Investigación Tecnológica (IIT), ETSI ICAI, Universidad Pontificia Comillas, 28015 Madrid, Spain; Javier.Renedo@iit.comillas.edu
* Correspondence: ahmadasrul@ukm.edu.my; Tel.: +60-3-89216591

Received: 14 September 2019; Accepted: 31 October 2019; Published: 3 November 2019

Featured Application: The proposed active network management framework with a flexible hybrid AC/DC distribution network topology allows for a secured operation during contingencies. Furthermore, the application of an integrated multi-terminal medium voltage DC (MVDC) helps to achieve a more efficient network operation, reduce demand interception, and encourage more contribution from renewable generations.

Abstract: A new active network management framework is presented based on a multi-period optimal power flow problem that is bounded by security constraints at the distribution level for upholding the security of supply. This can be achieved through active engagement with flexible demand and distributed generation to prepare for contingency events in day-ahead operational planning. This framework is coupled with a flexible hybrid AC/DC medium voltage (MV) distribution network topology. It contains an integrated multi-terminal medium voltage DC (MVDC) interface for a seamless interaction and integration of the flexible demand and generation on both AC and DC sides of the hybrid network. The active energy management framework when coupled with a flexible hybrid AC/DC topology provides unprecedented degrees of flexibility as well as security of operation under a variety of conditions. To this end, the 75-bus UK generic distribution network has been modified and converted into a hybrid AC/DC network using the integrated MVDC interface. This framework is then deployed to minimise operational costs to the network operator, considering costs of schemes such as distributed generation curtailment and flexible demand shifting, as well as network losses. Results show a significant improvement in operational costs when the network operates as a flexible hybrid when compared to a pure AC or a more conventional AC/DC hybrid.

Keywords: distribution-security optimal power flow; energy management; flexible demand and generation; integrated AC/DC system

1. Introduction

The global energy and environmental targets have directed most countries worldwide towards a greener energy generation portfolio. A large portion of renewable generation capacity is likely to be in form of distributed generations (DGs) directly connected to distribution (medium and low voltage) networks [1]. The increasing number of DGs, such as wind turbines and solar photovoltaic (PV) generators operating with an internal DC link has brought forward the concept of DC collector grids [2].

This concept is not limited to DGs integration as it can also be used as an interface for integrating DC loads such as electric vehicle's (EV) charging facilities, battery energy storage systems (BESS), LED lighting systems, DC data centers, and variable-speed machines. Furthermore, the DC system operates at a higher efficiency due to a reactive power that is not present, therefore reducing conduction losses. It is likely that the future medium voltage (MV) distribution network will consist of a hybrid AC/DC network or at least some parts of it. In recent years, there have been several demonstration projects of deployment of medium voltage DC (MVDC) networks. A campus project was developed by RWTH Aachen University to investigate the benefits of MVDC grids [3–5]. In the context of the UK, the first trial project of a MVDC link called "Angle-DC" will be installed by transforming the existing 33-kV AC distribution circuits between the Llanfair PG substation on Anglesey and the Bangor substation at North Wales [6] into DC operation.

The voltage source converter (VSC) is the key element in enabling the deployment of MVDC infrastructure in existing distribution networks. A back-to-back (BTB) configuration of VSCs has been introduced in [7] by replacing the normally open mechanical switches at the end of feeders, called soft-open point (SOP), to facilitate DG penetration in distribution networks. In a later study, [8] advocated the benefit of SOPs in terms of fault isolation and supply restoration. In [9], the SOP was suggested to replace all remotely controlled switches which include both tie switches and sectionalising switches for a rapid network reconfiguration. The capability of SOP for fast voltage regulation was investigated in [10]. Since the application of SOPs provides operational flexibility to distribution networks, it has been considered as one of the factors to determine an optimal placement for distributed energy storage in [11]. A dynamic energy management framework considering renewable generations, energy storage systems, flexible demands, and the SOP application was proposed in [12]. In a recent study, [13] introduced a decentralised control of VSC stations to address the issue of communication failure. Like the demonstration project in [6], these studies [7–13] only considered the interconnection between any two feeders which would limit control (e.g., load transfer capability) to the two feeders. In recent years, the multi-terminal high voltage direct current (HVDC) configurations have been investigated extensively at the transmission level [14–19]. A similar concept is plausible and may be applied at the MV level to achieve higher levels of operational flexibility by connecting all end feeders together.

This paper proposes a flexible hybrid AC/DC MV distribution grid concept, which at its core takes advantage of the higher levels of operational flexibility by using an integrated MVDC interface that consists of a DC collection grid containing multiple VSCs and connects all end feeders together. Consequently, all DGs with internal DC links (wind and solar generators) can be connected directly to the MVDC system. The MVDC interface may also be used to achieve power transfer between the feeders, improving voltage control (e.g., at end feeders) and improving the control of the power flows. This expands the application of soft-open points (SOP) to all feeders. Meanwhile, an active network management (ANM) framework is proposed in order to operate this hybrid network to its fullest potential. The ANM framework optimises the operation of multiple VSCs within the network and takes advantage of schemes such as flexible demand shifting and renewable energy curtailment to minimise operational costs and maintain a continuity of supply to all loads even after contingencies.

The concept of steady-state operational security is well known for transmission networks. However, a similar concept has received little attention for distribution networks, mostly due to the radial configuration of distribution feeders. Notwithstanding this, the problem of operational security in distribution networks has been introduced in [20]. The work in [20] proposed a distribution system security region (DSSR), based on the concept of total supply capability (TSC) [21]. In this way, all operating points were determined, satisfying the $N-1$ security criteria. The approach considered the capacities of substation transformers, network topology, and operational constraints. This concept was also applied in [22] at a varying load using network reconfiguration techniques to reduce total load shedding. Recently, a quantitative maximum DG output assessment was used in [23] based the concept of DSSR to guarantee the $N-1$ secure operation of distribution networks. The work

in [24] incorporated the situation awareness that involved three steps: Perception (i.e., data collection), comprehension (i.e., data analysis), and projection (i.e., data prediction) to carry out preventive actions toward any contingency events. However, the studies allow load interruptions during contingencies and lack of involvement from other network devices to react toward undesirable events. In our ANM framework, however, using the MVDC interface in conjunction with flexible demand and renewable energy curtailment entails that the operating of loads and grid supply points can be planned in advance (i.e., day-ahead) in such a way to keep the continuity of supply at contingency conditions given a $N-1$ criterion in place. We, therefore, introduce a new distribution security constrained optimal power flow (D-SCOPF) that contains three stages, namely pre-contingency, short-term, and long-term post-contingencies to distinguish from the DSSR. The short-term contingency period is introduced in order to take advantage of the fast control of VSCs connected to the MVDC interface and distinguish from other slow reaction devices such as the tap changer in the long-term contingency period.

Our contributions in this paper are three-fold: (1) A day-ahead distribution network management framework with flexible demand and DG curtailment to uphold the secure operation during contingencies, (2) an extended security constrained, which covers three stages, pre-contingency, short-term, and long-term post-contingencies, is used to highlight the different remedial action capabilities between slow response (i.e., load tap changer) and fast response (i.e., VSCs) control devices, and (3) a multi-terminal configuration of MVDC is introduced to alleviate the limitations of back-to-back (BTB) or point-to-point (P2P) configurations used in [7–13] and thus a more flexible network operation can be achieved. The MVDC interface works as a platform for renewable energy integrations at the end of distribution feeders that uses the same number of VSCs as in P2P configuration.

This paper is organised as follows: A new active network management by adopting the flexible demand and non-firm distributed generation for security operational is presented in Section 2, Section 3 describes a mathematical model of the hybrid AC/DC network for a possible application within the ANM framework, Section 4 discusses case studies and comparison results of applying the ANM framework to the hybrid network, and finally, a conclusion is drawn in Section 5.

2. A New Security ANM Framework

Typically, an ANM framework in distribution networks optimises the operation of the system without considering post contingency (faults) operational states [25]. The ANM framework proposed in this paper ensures a continuity of supply in the distribution network, even after the occurrence of faults in the feeders or substation transformers (satisfying the $N-1$ security criterion). The proposed ANM framework solves a multi-period D-SCOPF that ensures a continuity of supply by imposing operational constraints in both normal operation (pre-contingency) and abnormal (post-contingency) conditions [26]. The proposed ANM framework is to be operated by the distribution system operator (DSO). This requires a SCADA system with remote controllers. In this way, set points for control actions of the VSCs, DG curtailment, and demand shift will be provided by the centralised controller (ANM framework).

Figure 1 shows a flowchart of the introduced ANM framework where $\mathbf{x}$ is the vector of state variables (voltage magnitudes and angles), $\mathbf{u}$ is the vector of conventional control variables (tap changer operation), and $\mathbf{w}$ is the vector of the fast control variables (modulation index and phase shift of VSCs). The responses available to the DSO are divided into two time scales: short-term and long-term. Parameter α in Figure 1 is used to relax the limits of the equipment during the short-term time scale immediately after a contingency (commonly called emergency ratings). Immediately after a contingency, the fast response of the VSCs will provide short-term remedial actions, followed by long-term corrective actions carried out by slower devices such as tap changers. The proposed ANM framework is divided into four main layers and will be explained in the following subsections:

1. Load and generation forecasting;
2. Steady-state security assessment;

3. Distribution security-constrained optimal power flow;
4. Day-ahead optimal scheduling.

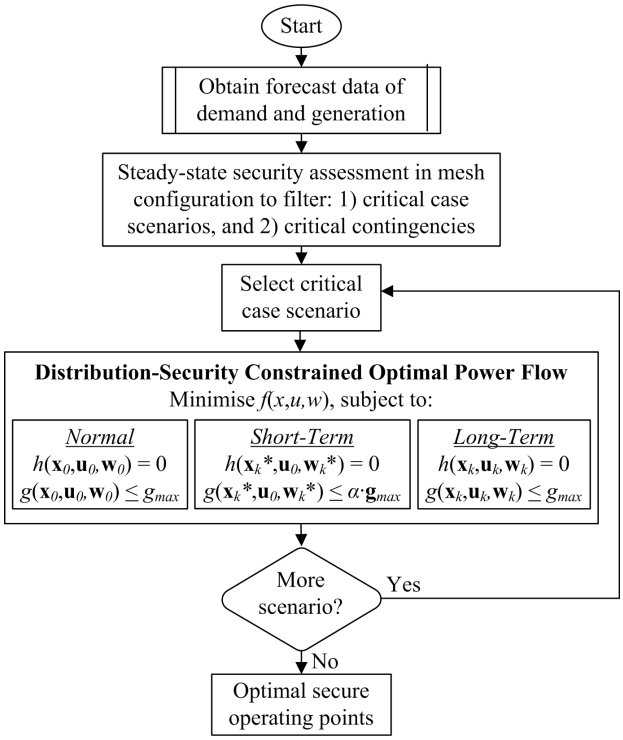

Figure 1. The flowchart of the introduced ANM (active network management) framework.

2.1. Load and Generation Forecasting

In the first layer, we assume the DSO has access to forecast data for load and generation profiles for the day-ahead time horizon. In this paper, we used historic data in [25] for our simulations.

2.2. Steady-State Security Assessment

The second layer consists of a steady-state security assessment where the critical contingencies from all scenarios obtained from demand and generation forecasting are identified. The critical contingency cases are selected from the contingency cases that cause violations of the operational constraints. The non-critical contingency cases are disregarded since they will not provide any difference in comparison to the conventional optimal power flow calculation. The critical contingency selection is carried out for all scenarios of demand and generation and therefore, identifying the critical case scenarios (i.e, demand and generation operating points binding with the critical contingency) can be done at the same time. The period of critical case scenarios is identified in a priori, in order to take into account effective control actions (i.e., power curtailment of the DGs and/or demand response). The objective of these control actions is to ensure that the system operational state always remains in the normal operation limits. This step is essential for reducing the number of contingency cases to be analysed and to identify the period of demand and generation operating points that affect the secure operation of the system. As a result, the size of the optimisation problem in the computational burden are reduced significantly.

An iterative procedure is proposed to identify the set of critical contingencies and case scenarios for each time period. The simulation is carried out in a meshed configuration (i.e., all tie switches are closed, in order to account for the worst conditions). Figure 2 shows the iterative procedure being used in this assessment to select the potential critical contingency cases. Let K be the set of contingencies used in the security analysis (i.e., line outages at the main feeders, including the transformers of

the main distribution substation) and let M_c be the set of critical case scenarios. Let $\boldsymbol{P}_{0\{m\}}$ be the optimal operating point at period $m \in M$. The proposed iterative procedure in Figure 2 can be further explained as follows:

1. Initialisation of the the critical contingency set and the subset of critical case scenario: $K_c = \emptyset$ and $M_c = \emptyset$;
2. Select a time period of the forecast demand and generation, $m \in M$, and solve an OPF using base case constraints. The optimal optimal operating point at period $m \in M$, obtained from the OPF is denoted as $\boldsymbol{P}_{0\{m\}}$;
3. Simulate each contingency $k \in K$ with $\boldsymbol{P}_{0\{m\}}$ by running a conventional power flow calculation. If the analysed contingencies do not lead to constraint violations, then $\boldsymbol{P}_{0\{m\}}$ is considered a secure optimal solution. Otherwise, the contingency case k that produces post-contingency violations of the limits is recorded as the subset of critical contingencies (K_c) and the time period of the forecast demand and generation, m is recorded in the subset of the critical case scenario (M_c);
4. The computation is continued for the next period and terminated after all periods $m \in M$ are executed.

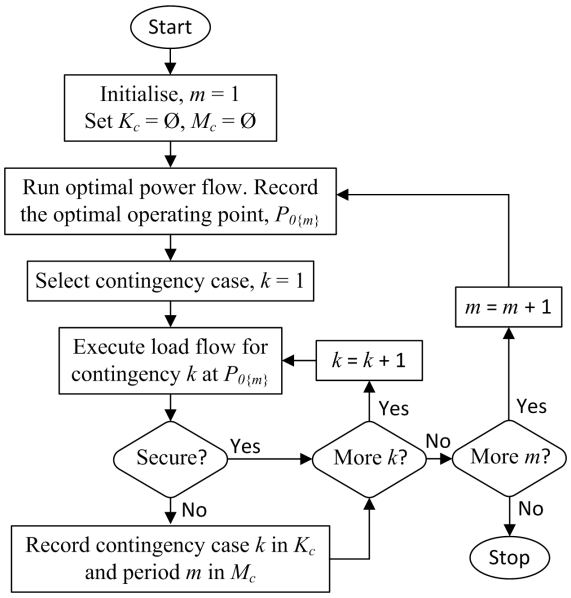

Figure 2. The flowchart of steady-state security assessment.

2.3. Distribution Security Constrained Optimal Power Flow

The third layer consists of solving a multi-period distribution security constrained optimal power flow (D-SCOPF) for the day-ahead time horizon. The secure optimum settings for preventive and corrective control actions (available to the DSO) will be obtained from the solution of the D-SCOPF. For the results presented in this paper, historic load/generation profiles will be used, rather than actual day-ahead time series values. Only the critical case scenarios (i.e., extreme cases of load/generation variations) will be considered in this layer in order to maintain computational efficiency. In this way, the D-SCOPF algorithm will run over the set of all binding contingencies for the selected critical case scenarios. Furthermore, the optimisation problem will be solved in three stages: Normal operation (pre-contingency), short-term, and long-term post-contingency, as shown in Figure 1.

The corrective controls are divided into short-term (VSC), long-term (LTC), and demand-shift, and DG curtailment. In the demand shift control scheme, a price π_{ds} will be paid to consumers in order to achieve the demand-shift services required by the DSO, P_{shift}. In the DG-curtailment scheme, a compensation price, π_{dg} is set. Therefore, the DSO will pay to the DG owners the required curtailed power, P_{curt}, at this price. The proposed D-SCOPF scheme also takes into account the cost

of power transfer losses, P_{loss}, at the forecast energy market price, π_{em}. It is assumed that $\pi_{ds} > \pi_{dg}$ because it is desirable to reduce the levels of demand shifting than the levels of DG power curtailment, in prioritising consumer welfare. Consequently, the objective function of the proposed D-SCOPF algorithm is formulated as:

$$F = \sum_{m \in M_c} \left[\sum_{w \in W} \pi^m_{dg} P^m_{curt\{w\}} + \sum_{b \in N} \pi^m_{ds} P^m_{shift\{b\}} + \sum_{l \in L} \pi^m_{em} P^m_{loss\{l\}} \right] \quad (1)$$

The details of the optimisation problems (power equations and constraints) are provided in Appendix A. This optimisation problem can be solved in the three stages: Normal operation (pre-contingency), short-term, and long-term post-contingency (refer Figure 1).

2.4. Day-Ahead Optimal Scheduling

In this layer, the final day-ahead optimal scheduling is generated for the DSO to share with other agents (i.e., DG owners, demand aggregators, and the upstream energy market operator). The offers/bids put forward by the DSO will obviously be based on the forecast prices used to create the final scheduling in the third layer.

3. A Hybrid AC/DC Topology

In this section, we first introduce a general overview of the MVDC interface circuit topology that is used to turn an AC distribution grid into a hybrid AC/DC system. The MVDC interface has been shown in Figure 3 and is used to provide a seamless connection between end feeders. In practice, the MVDC interface starts with a link between two substations as in the "Angle-DC" demonstration project [6] and then expands to the nearby substations to form a DC platform. The development progress is not necessarily continuous instead it can be done in stages as needed. This work is carried out to showcase the benefits to be gained after it forms the MVDC interface.

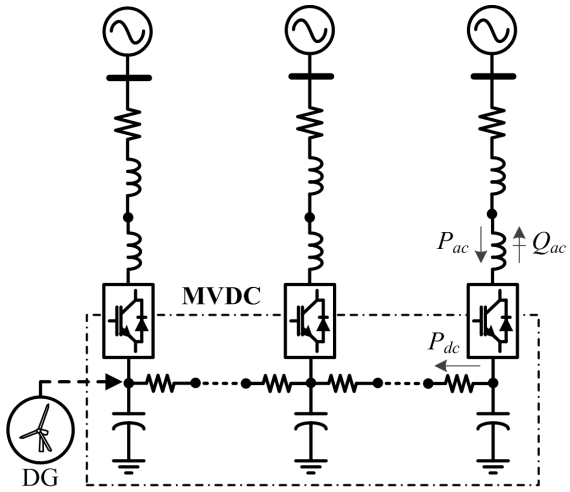

Figure 3. The MVDC (multi-terminal medium voltage DC) interface applied in a hybrid network

As mentioned in Section 1, the role of the MVDC interface is two-fold (i) to provide a platform for the seamless integration of DG resources with integrated DC links (e.g., MV wind parks or solar farms), as well as various types of typically DC flexible demand (e.g., electric vehicles, and battery storage systems) and (ii) to provide maximum operational flexibility through the extra levels of control afforded by the VSCs for improved voltage regulation as well as load balancing between feeders. This configuration guarantees the continuity of supply constraint. In the next sub-sections, the mathematical model of the MVDC system (to be included in the ANM framework) is described.

3.1. Unified VSC Model

Core to the MVDC interface model is the unified fundamental frequency model for the VSC which has already been introduced by us in [9,27,28]. The AC and DC sides of the VSC are coupled together through the following simple voltage relationship $V_{cr} = km_aE_{dc}$, essentially modelling the VSC in a fundamental frequency as an ideal transformer with a continuous complex tap ratio (m_a) signifying the pulse width modulation (PWM) control of a real VSC. The voltage relationship allows fo ther coupling of the AC and DC sides together for developing unified formulations of power flow equations for both the AC and DC sides of the converter and by extension for the hybrid network [9,27]. Consequently, the VSC control actions (i.e., AC power control and DC voltage control) may be modelled for power flows as well as optimal power flows on one unified frame of reference and solved simultaneously. The VSC model equivalent circuit as introduced in [9] is given in Figure 4.

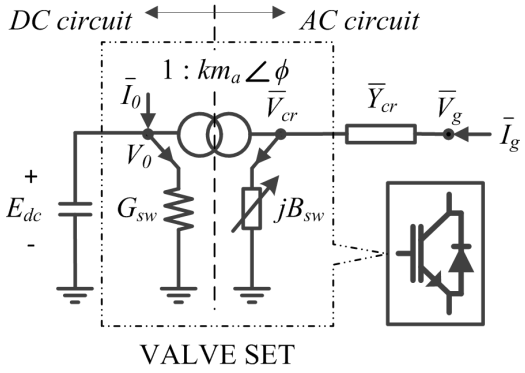

Figure 4. The equivalent VSC (voltage source converter) fundamental frequency model.

From Figure 4 the set of nodal current injections for the AC and DC sides of the converter are written as such:

$$\begin{bmatrix} \bar{I}_g \\ \bar{I}_0 \end{bmatrix} = \begin{bmatrix} \bar{Y}_{cr} & -km_a\bar{Y}_{cr}e^{j\phi} \\ -km_a\bar{Y}_{cr}e^{-j\phi} & G_{sw} + k^2m_a^2(\bar{Y}_{cr} + jB_{sw}) \end{bmatrix} \times \begin{bmatrix} \bar{V}_g \\ E_{dc} \end{bmatrix} \tag{2}$$

From Equation (2) we can then calculate the set of nodal power injections on both sides:

$$\begin{bmatrix} \bar{S}_g \\ \bar{S}_0 \end{bmatrix} = \begin{bmatrix} \bar{V}_g & 0 \\ 0 & E_{dc} \end{bmatrix} \begin{bmatrix} \bar{I}_g \\ \bar{I}_0 \end{bmatrix}^* \tag{3}$$

The nodal power injections at either side of the VSC, i.e., the bus g (AC side) and bus 0 (DC side) are calculated by expanding Equation (3) and knowing that the VSC is interfaced to the AC side by an equivalent phase reactor with admittance, $\bar{Y}_{cr} = j/x_{cr} = jB_{cr}$:

$$P_g = -B_{cr}km_aE_{dc}V_g\sin(\theta - \phi) \tag{4}$$

$$Q_g = -B_{cr}V_g^2 + B_{cr}km_aE_{dc}V_g\cos(\theta - \phi) \tag{5}$$

$$P_0 = G_{sw}E_{dc}^2 - B_{cr}km_aE_{dc}V_g\sin(\phi - \theta) \tag{6}$$

$$Q_0 = -(B_{cr} + B_{sw})k^2m_a^2E_{dc}^2 + B_{cr}km_aE_{dc}V_g\cos(\phi - \theta) \tag{7}$$

An additional constraint is imposed to ensure that reactive power injections into the DC buses are kept at zero:

$$-(B_{cr} + B_{sw})k^2m_a^2E_{dc}^2 + B_{cr}km_aE_{dc}V_g\cos(\phi - \theta) = 0 \tag{8}$$

where B_{sw} is an equivalent shunt susceptance at the AC side that models the reactive power injection/absorption of the converter.

Moreover, the shunt resistance of the VSC, G_{sw} is used to model the switching losses inside the converter. This term increases with the switching frequency of the PWM. When the VSC operates at a nominal current and rated DC voltage, the switching losses are represented with a constant conductance, G_0. Even though the DC voltage remains constant, the current injection changes according to the active and reactive power injections of the converter into the network. Therefore, the G_{sw} can be derived from the constant conductance and corrected by the quadratic of the operating current, I_{act} to the nominal current, I_{nom} as expressed in Equation (9) [27]:

$$G_{sw} = G_0 \left(\frac{I_{act}}{I_{nom}} \right)^2 \tag{9}$$

3.2. Unified Hybrid AC/DC Network Model

This section derives a unified model for steady-state analysis (conventional and optimal power flow calculation). The complete model consists of the VSCs and the AC/DC network. Figure 5 shows a feeder in the hybrid AC/DC network with the MVDC interface. The VSCs are represented using the unified modelling methodology presented in Section 3.1, while the network and the derivation of the complete model will be described in detail now.

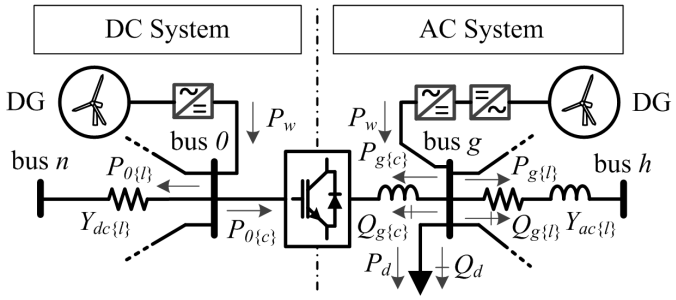

Figure 5. One feeder in the hybrid AC/DC network with the MVDC interface.

The entire hybrid AC/DC network will be modelled as a notionally only-AC system, as proposed in [29–31]. Specifically, the DC parts of the network are represented as notional only-AC parts, with resistive AC lines (zero reactance). This is possible due the equivalence of the power-flow equations of resistive AC lines in AC systems and the power-flow equations, as discussed in [28]. With this modelling approach, bus voltages and currents of the DC systems will be complex numbers, as those in AC systems, but with a zero imaginary part. Hence, the entire hybrid network, represented as a notionally only-AC equivalent system, will have an admittance matrix. Therefore, the nodal power-flow injections can be written with:

$$\boldsymbol{S} = diag(\boldsymbol{V}) \times (\boldsymbol{Y}^*_{acdc} \boldsymbol{V}^*) \tag{10}$$

where the vector $\boldsymbol{V}$ contains all nodal voltages (of the AC and DC systems) belonging to the set N and $\boldsymbol{Y}_{acdc}$ is the admittance matrix of the complete AC/DC system. The entire network can be modelled using Equation (10), as a notionally only-AC system by assuming that there is no reactance in the DC side. Meanwhile, the nodal power injections of the AC feeders can be written as (see Figure 5 and Equation (10)):

$$\overline{S}_{g\{l\}} = \overline{Y}_{ac\{l\}} [V_g^2 - \overline{V}_g \overline{V}^*_h] \tag{11}$$

The power balance equations of every AC feeder can be written as:

$$P_{g\{c\}} + \sum_{l=1}^{nl} P_{g\{l\}} + P_{d\{g\}} - P_{w\{g\}} = 0 \tag{12}$$

$$Q_{g\{c\}} + \sum_{l=1}^{nl} Q_{g\{l\}} + Q_{d\{g\}} = 0 \tag{13}$$

where nl is the total number of lines connected to bus g. The subscripts d and w refer to the loads and wind-based DGs at their respective buses.

Following Equation (10), the active and reactive power injections in the DC side can be written as:

$$P_{0\{l\}} = G_{dc\{l\}}[E^2_{dc\{0\}} - E_{dc\{0\}}E_{dc\{n\}}\cos(\theta_0 - \theta_n)] = G_{dc\{l\}}E_{dc\{0\}}\triangle E_{dc} \tag{14}$$

$$Q_{0\{l\}} = -E_{dc\{0\}}E_{dc\{n\}}G_{dc\{l\}}\sin(\theta_0 - \theta_n)] = 0 \tag{15}$$

In Equation (14) and (15), $\triangle E_{dc} = E_{dc\{0\}} - E_{dc\{n\}}$ and $Y_{dc\{l\}} = G_{dc\{l\}}$. By imposing the zero-reactive power injection condition, as expressed in Equation (8) and (15), the angles of the voltages of the DC buses will be zero $\theta_n = \theta_0 = 0$ (initial angles of zero are assumed). Therefore, the total nodal active power injection at bus 0 of the the DC side is given by:

$$\sum_{l=1}^{nl} P_{0\{l\}} = \sum_{l=1}^{nl} G_{dc\{l\}}E_{dc\{0\}}\triangle E_{dc} \tag{16}$$

And the power balance at bus 0 of the DC side reads:

$$P_{0\{c\}} + \sum_{l=1}^{nl} P_{0\{l\}} - P_{w\{0\}} = 0 \tag{17}$$

It follows from Equation (10) and from the assumptions on the DC side, that in the hybrid AC/DC network for any node, b, the total calculated power injections can be calculated as below, considering the nodal power injections for the converter and the MVDC feeder derived in Equation (4)–(7), Equation (11), as well as Equation (14)–(15), respectively:

$$\sum_{c\in C} P_{b\{c\}} + \sum_{l\in L} P_{b\{l\}} + P_{d\{b\}} - P_{w\{b\}} = 0 \qquad \forall b \in N \tag{18}$$

$$\sum_{c\in C} Q_{b\{c\}} + \sum_{l\in L} Q_{b\{l\}} + Q_{d\{b\}} = 0 \qquad \forall b \in N \tag{19}$$

This unified model can now be implemented in the proposed security ANM framework described in the earlier section.

4. Case Study and Results

The application of a hybrid AC/DC system with the proposed security ANM framework is now analysed in an urban UK distribution system. The application of the ANM framework is assessed based on minimum DG curtailment and demand shifting that could be achieved under relevant system contingencies.

The test system considered for this study consists of the 11-kV urban 77-bus UK generic system in [32] with a MVDC interface at the end of all feeders of the system, as shown in Figure 6. The distribution system is fed from a 33-kV utility grid through two substation transformers. The hybrid AC/DC distribution system contains 75 AC lines and 7 additional DC lines. Four of the DC lines are considered as the existing tie lines (marked with red solid lines). It is assumed that the system is supported by 23 wind-based DGs with a capacity of 1.73 MW each. The total peak load is

24.274 MW and 4.855 MVar. The off-peak load is considered at 40% of the peak load. The voltage limits are set to 0.97/1.03 p.u. (±3% of the nominal voltage) at all buses and thermal limits as given in [32] are used in this study. These limits are relaxed at short-term emergency ratings of 0.94/1.06 p.u. at all bus voltages and thermal limits are 20% higher than the continuous current ratings of the original case.

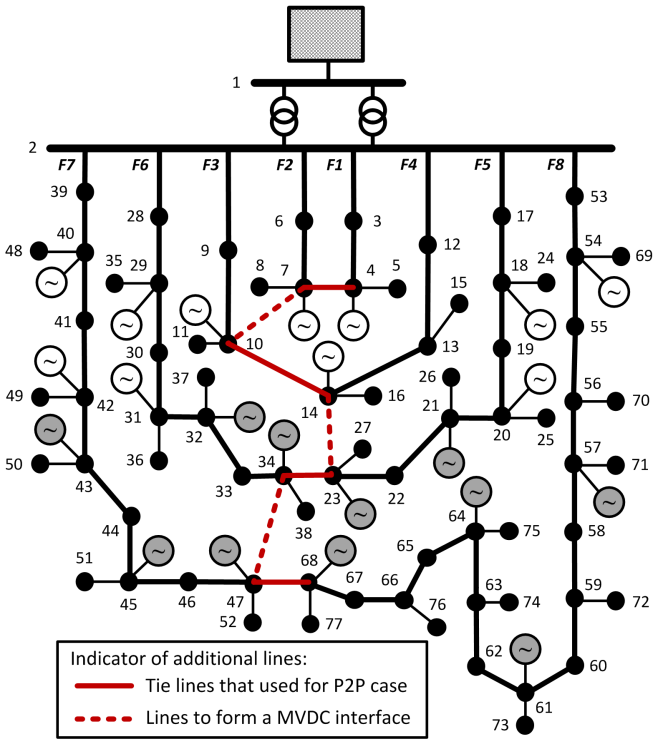

Figure 6. The modified hybrid AC/DC UK generic distribution system.

The parameter of the VSCs are provided in Table 1. The demand and generation profiles were obtained from the historic demand and wind data of central Scotland in 2003, as presented in [25]. The data contain two sets of wind generation profiles (as a percentage of the total generation capacity) and one set of demand profile (as a percentage of the system peak load). The number of coincident hours per year for each condition that occurred in the year is also provided. In this study, we have chosen a subset of the original data used containing only instances of high-generation low-demand and low-generation high-demand for our simulation purposes. The selected critical case scenarios of demand and generation profiles are described in Table 2.

Table 1. Converter parameter settings.

Item	Parameter Settings
VSC rating	5 MVA
DC voltage	±33 kV
Phase reactor, x_{cr}	0.1 p.u.
Constant conductance, G_0	0.01 p.u.

Table 2. Critical case scenarios obtained from [25].

No.	Wind 1 (%)	Wind 2 (%)	Load (%)	No. of hours
1	0	0	70	114
2	0	0	80	78
3	0	0	90	39
4	0	0	100	2
5	0	10	80	49
6	0	10	90	14
7	10	10	80	238
8	10	10	90	100
9	10	10	100	8
10	10	20	90	56
11	10	20	100	3
12	20	20	90	22
13	20	20	100	6
14	20	30	100	8
15	100	0	80	10
16	100	0	90	11
17	70	90	50	16
18	80	90	50	48
19	80	100	60	18
20	90	100	40	2
21	90	100	50	54
22	90	100	60	144
23	90	100	70	212
24	100	100	50	63
25	100	100	60	249
26	100	100	70	555

As described earlier in Section 2, we ran a steady-state security assessment for the original test system (without modifications) to identify all the binding contingencies. Since historic data was used, we only considered the critical case scenarios given in Table 2. For the original UK generic system, there are 19 critical contingency cases given in Table 3. We considered these for the modified hybrid network as well. From Table 3, it is clearly shown that outages of any line in the short feeders (F1 to F4) and tie-lines are non-binding.

Table 3. Critical contingency cases.

Feeders	Outages (lines)
F5	2–17, 17–18, 18–19, and 19–20
F6	2–28, 28–29, 29–30, and 30–31
F7	2–39, 39–40, 40–41, and 41–42
F8	2–53, 53–54, 54–55, 55–56, 56–57, 57–58, and 58–59

Three configurations are considered:

- Base case: Original AC configuration;
- Point-to-point (P2P): VSCs are installed at end of the tie lines with P2P configuration, as proposed in [6,13];
- MVDC: Modified hybrid configuration, where the MVDC interface acts as a platform for all DGs with internal DC links and loads, as shown in Figure 5. The MVDC configuration is an extension of use of DC links in [6,13], using the same number of VSC stations.

The base case does not contain VSCs and, therefore, the only control actions available to the DSO are the LTC voltage control, DG curtailment, and flexible demand shifting. In both, P2P and MVDC configurations, all available active network management schemes in the base case are used, in addition to the control actions of the VSCs. The D-SCOPF algorithm described in Section 2 has been implemented in AIMMS [33]. The optimisation problem is solved using CONOPT 3.14V on a PC of 3.5 GHz and 8 GB RAM. The performances of the three configurations are compared in terms of operating costs, demand shift, DG curtailment, line power loadings, and tap ratio optimal settings.

4.1. Operating Costs

Comparison results of the three configurations (base case, P2P, and MV) are provided in Table 4. The application of VSCs increased the total losses of the system, since the switching action in the VSCs introduced additional losses. Nevertheless, the use of VSCs, either in P2P or MVDC configurations, improved performance, reduced the shifted demand and DG curtailment, in comparison to the base case. When using the proposed MVDC interface, the curtailed energy was dramatically reduced by almost 3.5 in comparison to the base case and twice in comparison to the P2P configuration. Overall, results of Table 4 proves that, using the MVDC configuration, the DSO could save over 80% of operational costs in comparison to the base case while improving the continuity of the supply condition.

Table 4. A comparison in minimising the operation cost.

Item	System Configurations		
	Base Case	**P2P**	**MVDC**
System losses (MWh)	484.90	546.22	494.22
Demand shifted (MWh)	2161.82	576.43	445.78
Generation curtailed (MWh)	2174.66	1125.83	620.28
Operational cost ($)	88,611.79	25,425.09	16,658.25
Total cost reduction	-	71.3%	81.2%

4.2. Demand Shift

Figures 7 and 8 show the percentage of maximum demand shift for the analysed three system configurations. The largest demand shift occurred during a period of high demand and low generation (load at 100% of peak demand and both wind generations are 0%), as shown in Figure 7. However, this scenario did not appear very often as shown in Figure 8. Results showed that a demand shift of 73.9% in the base case could be reduced to 49.3% (with the P2P configuration) and to 46.7% (with the MVDC configuration). Hence, the MVDC configuration presented the best performance. This particularly can also be observed in Figure 8, where maximum demand shift using P2P configuration was between 30%–45%, while it was reduced significantly to 25%–40%, when using the proposed MVDC configuration.

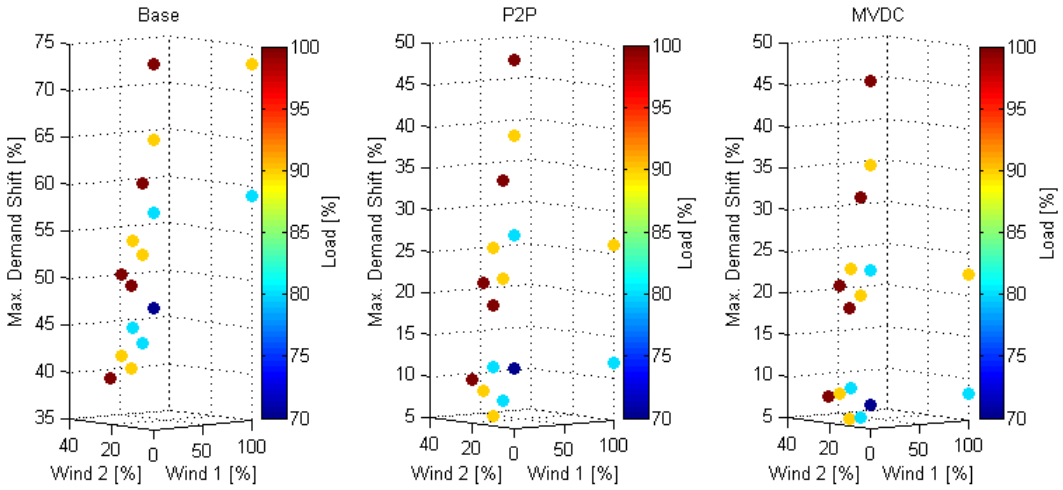

Figure 7. The comparison of maximum demand shift at different system configurations.

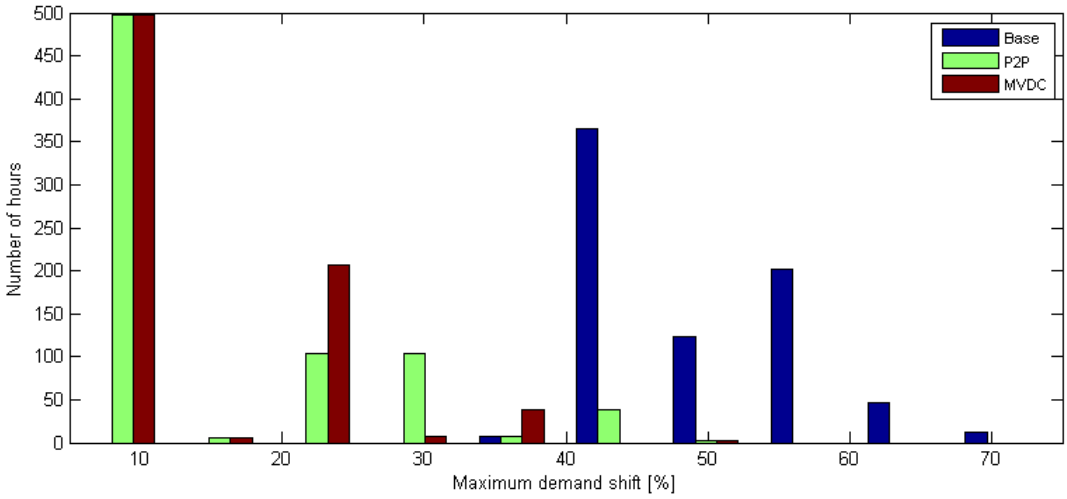

Figure 8. The distribution of maximum demand shift within the study period.

4.3. DG Curtailment

In scenarios with low demand and high generation, the power curtailment of DG takes place. Figures 9 and 10 show the total DG power curtailment for the analysed three configurations. The highest total DG power curtailment occurred in the base case (5.03 MW), as shown in Figure 9. With P2P configuration, DG power curtailment was reduced to 4.29 MW (a reduction of 15%) and DG power curtailment with the proposed MVDC interface was reduced to 2.05 MW (a substantial reduction of 59% was achieved). Furthermore, the DG curtailment was at a minimum when using the proposed MVDC configuration, as illustrated in Figure 10. Results clearly proved that the application of the proposed MVDC interface maximised the usage of renewable DG resources in the distribution network.

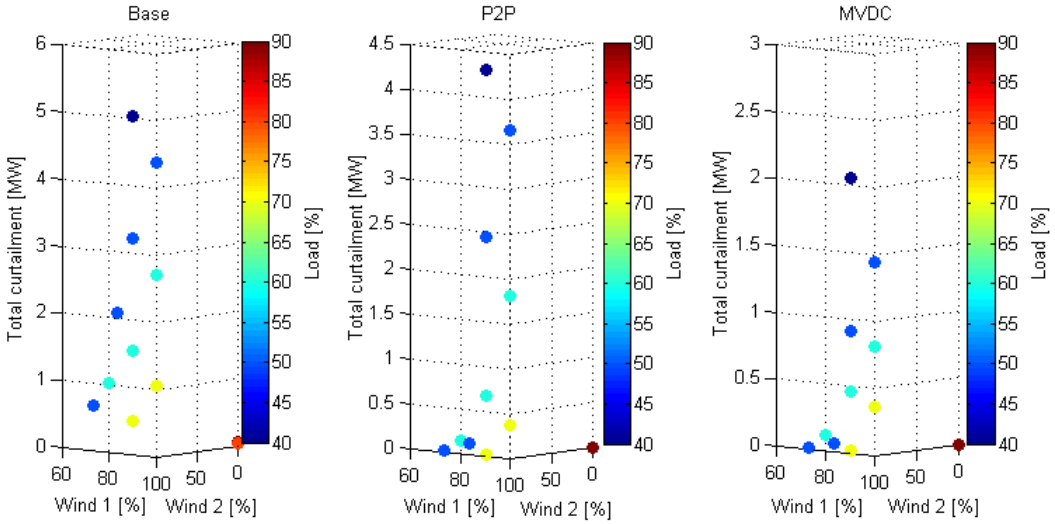

Figure 9. The comparison of total DG curtailment at different system configurations.

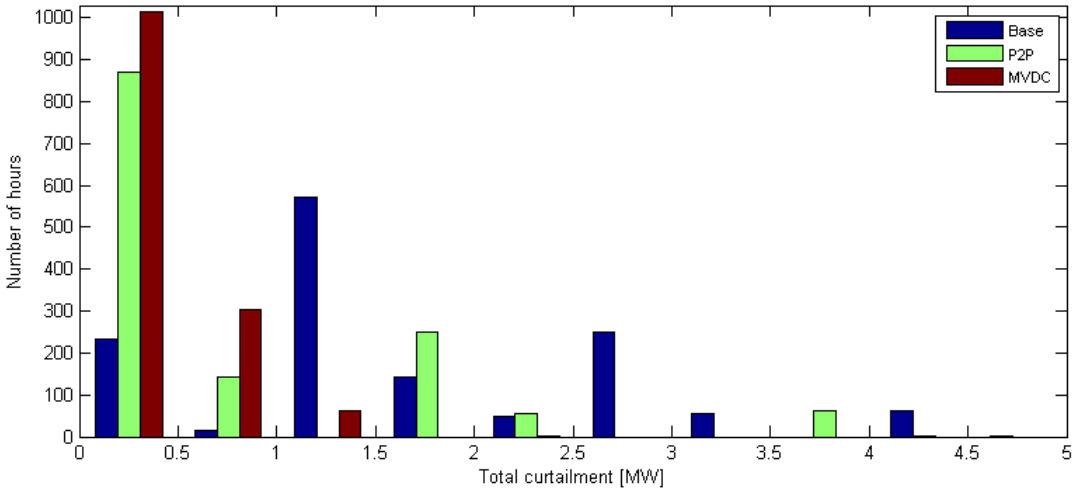

Figure 10. The distribution of total DG curtailment within the study period.

4.4. Line Loading

Figure 11 shows the deviations of the power flow through the line with the highest power loading, obtained with P2P and MVDC configurations. Deviations were calculated with respect to the power flow of the base case: △line loading (%) = selected case loading (%) − base case loading (%). Results show that P2P configuration presented a much higher line power loading than the base case, in order to maximise the DG usage as well as demand shift. On the other hand, MVDC configuration not only presented lower DG curtailment and demand shift (as shown in previous subsection), but it also maintained the low line power loading during high demand (scenarios 1–16) and further decreased the loading during high DG output (scenarios 17–26). This was due to the fact that the MVDC interface allowed a power exchange between multiple feeders.

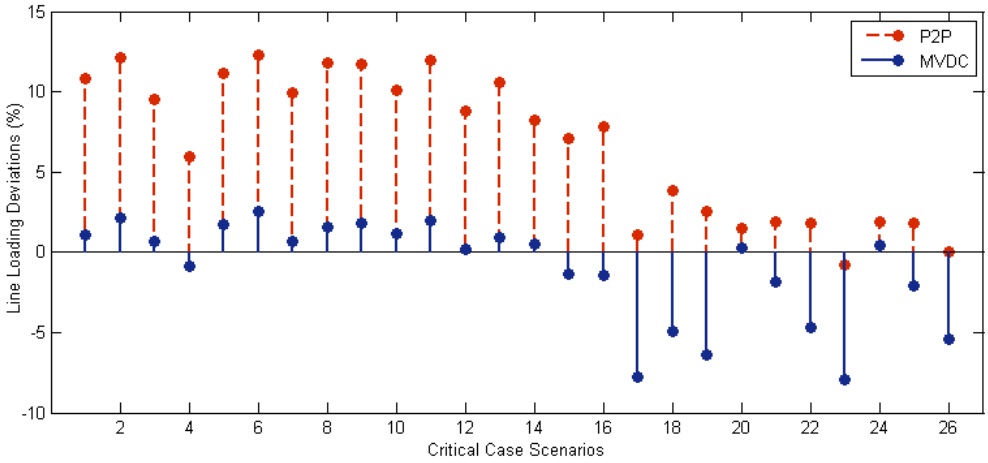

Figure 11. The comparison of loading deviations from the base case.

4.5. Tap Ratio Setting

Figure 12 shows the deviation of the tap ratio at the substation transformers, obtained in all 26 critical case scenarios, in comparison to the average tap settings. The deviation of the tap ratio was calculated for each of the analysed three configurations (base case, P2P, and MVDC) and was calculated as: $\triangle r = r - \bar{r}$. The average of the tap settings, $\bar{r}$ obtained in the base case, with P2P configuration and with MVDC configuration were 1.029, 1.025, and 1.029, respectively. In all three configurations, tap ratios operated at higher values of r during high-demand at low DG generation (scenarios 1–16 of Table 2) in comparison to the scenarios with lower demand and higher DG generation (scenarios 17–26 of Table 2). The base case presents the highest deviations of the tap ratio and less tap ratio deviations obtained with the hybrid configurations (P2P and MVDC). This was because the VSCs in the hybrid AC/DC system could provide fast remedial actions of reactive power support, especially during short-term periods. The MVDC configuration presents the least deviations due to the active power transfer flexibility between multiple feeders through the MVDC network.

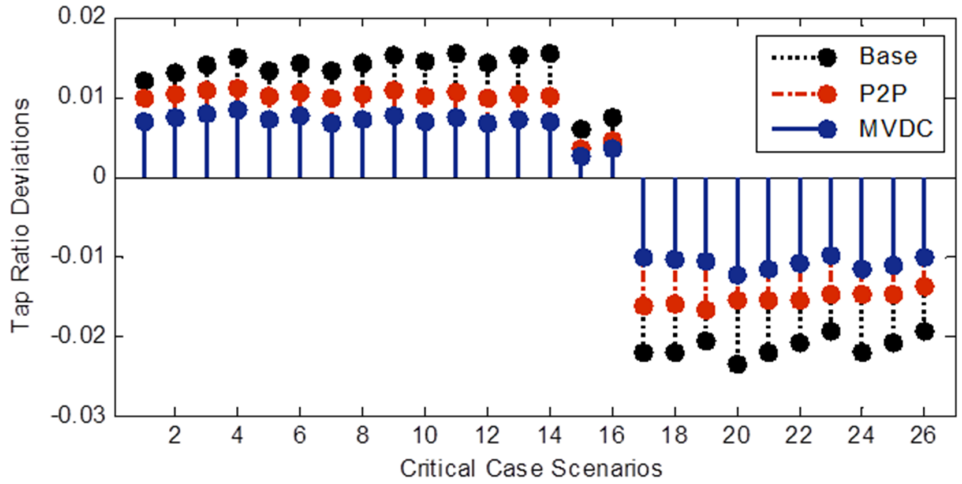

Figure 12. The comparison of tap ratio deviations at different case studies.

4.6. Investment Costs and Revenue

Notwithstanding the fact that the scope of this paper is on evaluating the impact of short-term operational planning cost savings of the MVDC interface when compared to individual P2Ps, a simple cost analysis was carried out to evaluate the operational cost savings in Table 4, weighing against the initial investment cost of the MVDC implementation. Investment costs to build SOP and

new distribution lines have been estimated in [34] as given in Appendix B. Referring to Table A1, the investment cost for two VSC stations in back-to-back configuration (i.e., SOP) is £90,000 or approximately $57,000 per VSC station and the cost for a new line installation is £65,000/km or approximately $131,000 per mile in length. We assume the distance between feeders is around half a mile for the additional lines and make use of the existing tie lines to form a MVDC interface in this study. Table 5 presents an estimated investment cost and return on the investment for the analysed configurations. A net present value (NPV) for the revenue generated from each technology is calculated from the total operational cost savings during period t (denoted as $Revenue_t$) and the total initial investment cost (denoted as $Investment_0$) using the expression in Equation (20) with an interest rate, dr at 5%. The first year operational savings of the P2P and MVDC configurations can obtained from the difference between operational cost of the base case and the analysed configuration in Table 4. The operational costs are expected to increase over the years (due to inflation) and therefore, total operational cost savings vary at period t. For simplicity, we consider the operational costs increased in proportion to the interest rate, dr, and the lifetime of the invested technologies, $T = 30$. As shown in Table 5, the NPV at 30 years for the MVDC configuration is higher than the P2P configuration, which means MVDC is more profitable. The payback period is also presented in Table 5, obtained when the NPV = 0 (i.e., total revenue equals to the investment cost). It is clearly shown that the MVDC configuration requires less than two additional years as compared to the P2P configuration in order to get payback from the total investment cost. This indicates that the implications on the investment cost are not drastic and can be compensated with the potential technical benefits that can be gained in terms of demand shifting, DG power curtailment, line loadings, and tap ratio settings as discussed earlier.

$$\text{NPV} = \sum_{t=1}^{T} \frac{Revenue_t}{(1+dr)^t} - Investment_0 \tag{20}$$

Table 5. An estimated investment cost and return on investment.

Item	Hybrid Network Configurations	
	P2P	**MVDC**
Total VSC station cost	$456,000	$456,000
Total power lines cost	-	$196,500
Total investment cost	$456,000	$652,500
The NPV at 30 year	$1,349,334	$1,403,315
Payback period	7.6 years	9.5 years

5. Conclusions

This paper proposed a new security ANM framework for optimal operational planning in active distribution networks using a flexible hybrid VSC-based AC/DC system (containing MVDC interfaces) while upholding a security of supply condition. The proposed (ANM) scheme was described and applied to a modified urban 75-bus UK generic distribution network. The proposed ANM scheme was compared using three configurations: Base case (only AC), P2P (with point-to-point VSCs), and with the proposed configuration (MVDC). The advantage of the ANM framework was that it could guarantee a security of supply at all times akin to the reliability criterion applied to transmission systems (i.e., $N-1$).

The results clearly proved that the proposed approach with the proposed hybrid AC/DC configuration improved the operation of the distribution system. The proposed MVDC configuration reduced demand shifting and DG curtailment when compared to normal AC or hybrid P2P configurations while upholding continuity of supply. The MVDC interface also reduced the power loadings of the lines and facilitated the tap changer operation burden, since it provided seamless load

balancing between multiple feeders. The use of the proposed MVDC interface also showed significant savings to the DSO, when compared to the P2P configuration with the same number of VSCs.

Nevertheless, further work could be carried out to estimate the exact geographical locations of the MVDC placements. This is however highly dependent on specific networks and the topological and geographical constraints.

Author Contributions: Conceptualisation, A.A.I. and B.K.; methodology, A.A.I., B.K., and J.R.; validation, B.K. and J.R.; formal analysis and investigation, A.A.I.; writing–original draft preparation, A.A.I. and B.K.; writing–review and editing, A.A.I., B.K., and J.R.; supervision and project administration, B.K.; funding acquisition, A.A.I.

Funding: Ahmad Asrul Ibrahim was funded by Universiti Kebangsaan Malaysia through projects GGPM-2019-031 and GUP-2018-024. The work of Javier Renedo was supported by Madrid Regional Government through projects PRICAM-CM (Ref. S2013/ICE-2933) and PROMINT-CM (Ref. S2018/EMT-4366). The APC was funded by GUP-2018-024.

Conflicts of Interest: The authors declare no conflict of interest.

Nomenclature

Abbreviations

AC	Alternating current
ANM	Active network management
BESS	Battery energy storage system
BTB	Back-to-back
DC	Direct current
DG	Distributed generation
D-SCOPF	Distribution security constrained optimal power flow
DSO	Distribution system operator
DSSR	Distribution system security region
EV	Electric vehicle
HVDC	High voltage direct current
LTC	Load tap changer
MV	Medium voltage
MVDC	Medium voltage direct current
NPV	Net present value
OPF	Optimal power flow
P2P	Point-to-point
PWM	Pulse width modulation
PV	Photovoltaic
SCADA	Supervisory control and data acquisition
TSC	Total supply capability
VSC	Voltage source converter

Notations

x	state variables (i.e., voltage magnitudes and angles)
u	conventional control variables (i.e., tap changer)
w	fast control variables (i.e., modulation index and angle of VSC)
π_{ds}	payment price for demand shifting
π_{dg}	payment price for DG curtailment
π_{em}	an electricity market price
ξ_b	demand shifting factor at bus b
m_a	modulation index
E_{dc}	voltage at DC side of VSC terminal
V_{cr}	voltage at AC side of VSC terminal
V_g	AC voltage at the connected grid of VSC

Y_{cr}	equivalent VSC interfaced admittance
B_{sw}	equivalent VSC switching shunt susceptance
G_{sw}	equivalent VSC switching conductance
P_{loss}	active power loss
P_w	active power output of DG unit
P_{curt}	curtailed active power of DG output
P_{shift}	shifted active power of demand
P_d, Q_d	active and reactive power consumption
P_g, Q_g	active and reactive power injections at AC connected bus of VSC
P_0, Q_0	active and reactive power injections at DC connected bus of VSC

Appendix A

Let N, W, G, L, O, C, K, and M denote the sets of respectively, nodes, wind power units, grid supply points (GSP), power lines, the subset of lines with on-load tap changer (OLTC) transformers, the subset of lines with BTB-VSCs, operating states and time periods. The full optimal operation planning in period $m \in M$ is formulated as a full AC optimal power flow problem as below:

$$P_g^{min} \leq P_g^m \leq P_g^{max} \quad \forall g \in G \tag{A1}$$

$$Q_g^{min} \leq Q_g^m \leq Q_g^{max} \quad \forall g \in G \tag{A2}$$

$$0 \leq P_w^m \leq P_{ava\{w\}}^m \quad \forall w \in W \tag{A3}$$

$$\xi_b^{min} \leq \xi_b^m \leq \xi_b^{max} \quad \forall b \in N \tag{A4}$$

$$r_o^{min} \leq r_o^m \leq r_o^{max} \quad \forall o \in O \tag{A5}$$

$$V_g^m = 1 \quad \forall g \in G \tag{A6}$$

$$\theta_g^m = 0 \quad \forall g \in G \tag{A7}$$

$$V_{min} \leq V_b^m \leq V_{max} \quad \forall b \in N \tag{A8}$$

$$\overline{Y}_l \overline{Y}_l^* (\overline{V}_{rn\{l\}}^m - \overline{V}_{sn\{l\}}^m)(\overline{V}_{rn\{l\}}^m - \overline{V}_{sn\{l\}}^m)^* \leq I_{max}^2 \quad \forall l \in L \tag{A9}$$

$$\overline{Y}_{cr} \overline{Y}_{cr}^* (\overline{V}_{cr\{c\}}^m - \overline{V}_{sn\{c\}}^m)(\overline{V}_{cr\{c\}}^m - \overline{V}_{sn\{c\}}^m)^* \leq I_{nom}^2 \quad \forall c \in C \tag{A10}$$

$$Q_{0\{c\}}^m) = 0 \quad \forall c \in C \tag{A11}$$

$$P_{g\{b\}}^m + P_{w\{b\}}^m = \xi_b^m(P_b^m) + \sum_{l \in L} P_{b\{l\}}^m + \sum_{c \in C} P_{b\{c\}}^m \quad \forall b \in N \tag{A12}$$

$$Q_{g\{b\}}^m = \xi_b^m(Q_b^m) + \sum_{l \in L} Q_{b\{l\}}^m + \sum_{c \in C} Q_{b\{c\}}^m \quad \forall b \in N \tag{A13}$$

Equation (A1) and (A2) represent the limits of the active and reactive power flows through the primary substation transformer (i.e., the grid supply point). Equation (A3) represents the operating limits of DGs (wind generators), whereas Equation (A4) represents the limits of the demand shifting factor ξ. The demand shifting factor is defined as the proportion of demand that can be shifted at any time. Equation (A5)–(A7) represent the limits on the tap changer ratio, and the magnitude and phase angle of the voltage at the grid supply point. Equation (A8) represents bus-voltage limits. Equation (A9) and (A10) represent the thermal operating limits on lines and the converters (current limits). In these constraints, $\{sn, rn, cr\} \in N$ are the sending and receiving ends of a line and the corresponding VSC-connected buses, respectively. It should be pointed out that as per the operating requirements limit Equation (A9) may be relaxed for short-term post-fault periods. Equation (A11) represents the zero-reactive power limit into the the DC sides of the VSCs. Finally, Equation (A12) and (A13) represent the total nodal power balance equations at every bus, b (regardless of AC or DC). For simplicity purposes, only equations for pre-fault state, $k = 0$, have been described but the proposed D-SCOPF algorithm contains the constraints for all states, $k \in K$.

Appendix B

The estimated investment cost for the respective technologies used in this work according to [34] is shown in the following table:

Table A1. The available technologies for investment. [34]

Technology	Build Time (epochs)	Investment Cost
Soft open point	0	£90,000
Reconductoring	1	£65,000/km

References

1. Green, T.; Silversides, R.; Lüth, T. *Power Electronics in Distribution System Management*; Technical Report; HubNet Position Paper Series; The Supergen Energy Networks Hub: Newcastle upon Tyne, UK, 2015.
2. Siddique, H.A.B.; Doncker, R.W.D. Evaluation of DC Collector-Grid Configurations for Large Photovoltaic Parks. *IEEE Trans. Power Deliv.* **2018**, *33*, 311–320, doi:10.1109/TPWRD.2017.2702018.
3. Mura, F.; Doncker, R.W.D. Design aspects of a medium-voltage direct current (MVDC) grid for a university campus. In Proceedings of the 8th International Conference on Power Electronics—ECCE Asia, Jeju, Korea, 30 May–3 June 2011; pp. 2359–2366, doi:10.1109/ICPE.2011.5944508.
4. Stieneker, M.; Butz, J.; Rabiee, S.; Stagge, H.; Doncker, R.W.D. Medium-Voltage DC Research Grid Aachen. In *International ETG Congress 2015*; Die Energiewende—Blueprints for the New Energy Age; VDE-Verlag: Berlin, Germany, 2015; pp. 1–7.
5. Stieneker, M.; Doncker, R.W.D. Medium-voltage DC distribution grids in urban areas. In Proceedings of the 2016 IEEE 7th International Symposium on Power Electronics for Distributed Generation Systems (PEDG), Vancouver, BC, Canada, 27–30 June 2016; pp. 1–7, doi:10.1109/PEDG.2016.7527045.
6. Yu, J.; Smith, K.; Urizarbarrena, M.; MacLeod, N.; Bryans, R.; Moon, A. Initial designs for the ANGLE DC project; Converting existing AC cable and overhead line into DC operation. In Proceedings of the 13th IET International Conference on AC and DC Power Transmission (ACDC 2017), Manchester, UK, 14–16 February 2017; pp. 1–6, doi:10.1049/cp.2017.0002.
7. Bloemink, J.M.; Green, T.C. Benefits of Distribution-Level Power Electronics for Supporting Distributed Generation Growth. *IEEE Trans. Power Deliv.* **2013**, *28*, 911–919, doi:10.1109/TPWRD.2012.2232313.
8. Cao, W.; Wu, J.; Jenkins, N.; Wang, C.; Green, T. Operating principle of Soft Open Points for electrical distribution network operation. *Appl. Energy* **2016**, *164*, 245–257.
9. Ibrahim, A.A.; Kazemtabrizi, B.; Dent, C. Operational planning and optimisation in active distribution networks using modern intelligent power flow controllers. In Proceedings of the 2016 IEEE PES Innovative Smart Grid Technologies Conference Europe (ISGT-Europe), Ljubljana, Slovenia, 9–12 October 2016; pp. 1–6, doi:10.1109/ISGTEurope.2016.7856196.
10. Li, P.; Ji, H.; Wang, C.; Zhao, J.; Song, G.; Ding, F.; Wu, J. Coordinated Control Method of Voltage and Reactive Power for Active Distribution Networks Based on Soft Open Point. *IEEE Trans. Sustain. Energy* **2017**, *8*, 1430–1442, doi:10.1109/TSTE.2017.2686009.
11. Bai, L.; Jiang, T.; Li, F.; Chen, H.; Li, X. Distributed energy storage planning in soft open point based active distribution networks incorporating network reconfiguration and DG reactive power capability. *Appl. Energy* **2018**, *210*, 1082–1091, doi:10.1016/j.apenergy.2017.07.004.
12. Zhu, Z.; Liu, D.; Liao, Q.; Tang, F.; Zhang, J.J.; Jiang, H. Optimal Power Scheduling for a Medium Voltage AC/DC Hybrid Distribution Network. *Sustainability* **2018**, *10*, 318, doi:10.3390/su10020318.
13. Han, C.; Song, S.; Kim, J.; Jang, G. Enhancing Line Capacity Utilization in Power Transmission System Using Active MVDC Link. *Energies* **2019**, *12*, 1589, doi:10.3390/en12091589.
14. Hannan, M.A.; Hussin, I.; Ker, P.J.; Hoque, M.M.; Hossain Lipu, M.S.; Hussain, A.; Rahman, M.S.A.; Faizal, C.W.M.; Blaabjerg, F. Advanced Control Strategies of VSC Based HVDC Transmission System: Issues and Potential Recommendations. *IEEE Access* **2018**, *6*, 78352–78369, doi:10.1109/ACCESS.2018.2885010.
15. Castro, L.M.; Acha, E.; Rodriguez-Rodriguez, J.R. Efficient method for the real-time contingency analysis of meshed HVDC power grids fed by VSC stations. *IET Gener. Transm. Distrib.* **2018**, *12*, 3158–3166, doi:10.1049/iet-gtd.2017.1104.

16. Linke, F.; Sass, F.; Westermann, D. Preventive Parameterization of DC Voltage Control for N-1 Security of AC-HVDC-systems. In Proceedings of the 2018 Power Systems Computation Conference (PSCC), Dublin, Ireland, 11–15 June 2018; pp. 1–7, doi:10.23919/PSCC.2018.8442868.
17. Yazdi, S.S.H.; Milimonfared, J.; Fathi, S.H.; Rouzbehi, K. Optimal placement and control variable setting of power flow controllers in multi-terminal HVDC grids for enhancing static security. *Int. J. Electr. Power Energy Syst.* **2018**, *102*, 272–286, doi:10.1016/j.ijepes.2018.05.001.
18. Hwang, S.; Song, S.; Jang, G.; Yoon, M. An Operation Strategy of the Hybrid Multi-Terminal HVDC for Contingency. *Energies* **2019**, *12*, 2042, doi:10.3390/en12112042.
19. Wen, Y.; Chung, C.Y.; Shuai, Z.; Che, L.; Xiao, Y.; Liu, X. Towards Flexible Risk-Limiting Operation of Multi-Terminal HVDC Grids with Vast Wind Generation. *IEEE Trans. Sustain. Energy* **2019**, doi:10.1109/TSTE.2019.2940488.
20. Xiao, J.; Gu, W.; Wang, C.; Li, F. Distribution system security region: Definition, model and security assessment. *IET Gener. Transm. Distrib.* **2012**, *6*, 1029–1035, doi:10.1049/iet-gtd.2011.0767.
21. Xiao, J.; Liang, H.S.; Xu, B.S.; Zhou, C.X.; Zhang, P. Study on weak link for distribution network based on total supply capability. In Proceedings of The 7th International Power Electronics and Motion Control Conference, Harbin, China, 2–5 June 2012; Volume 2, pp. 1469–1472, doi:10.1109/IPEMC.2012.6259041.
22. Chen, K.; Wu, W.; Zhang, B.; Djokic, S.; Harrison, G.P. A Method to Evaluate Total Supply Capability of Distribution Systems Considering Network Reconfiguration and Daily Load Curves. *IEEE Trans. Power Syst.* **2016**, *31*, 2096–2104, doi:10.1109/TPWRS.2015.2444792.
23. Liu, J.; Cheng, H.; Zeng, P.; Yao, L. Rapid assessment of maximum distributed generation output based on security distance for interconnected distribution networks. *Int. J. Electr. Power Energy Syst.* **2018**, *101*, 13 – 24, doi:10.1016/j.ijepes.2018.03.018.
24. Xiao, J.; Zhang, B.; Luo, F. Distribution Network Security Situation Awareness Method Based on Security Distance. *IEEE Access* **2019**, *7*, 37855–37864, doi:10.1109/ACCESS.2019.2906779.
25. Capitanescu, F.; Ochoa, L.F.; Margossian, H.; Hatziargyriou, N.D. Assessing the Potential of Network Reconfiguration to Improve Distributed Generation Hosting Capacity in Active Distribution Systems. *IEEE Trans. Power Syst.* **2015**, *30*, 346–356, doi:10.1109/TPWRS.2014.2320895.
26. Capitanescu, F.; Ramos, J.M.; Panciatici, P.; Kirschen, D.; Marcolini, A.M.; Platbrood, L.; Wehenkel, L. State-of-the-art, challenges, and future trends in security constrained optimal power flow. *Electr. Power Syst. Res.* **2011**, *81*, 1731 – 1741.
27. Kazemtabrizi, B.; Acha, E. An Advanced STATCOM Model for Optimal Power Flows Using Newton's Method. *IEEE Trans. Power Syst.* **2014**, *29*, 514–525, doi:10.1109/TPWRS.2013.2287914.
28. Renedo, J.; Ibrahim, A.A.; Kazemtabrizi, B.; García-Cerrada, A.; Rouco, L.; Zhao, Q.; García-González, J. A simplified algorithm to solve optimal power flows in hybrid VSC-based AC/DC systems. *Int. J. Electr. Power Energy Syst.* **2019**, *110*, 781–794, doi:10.1016/j.ijepes.2019.03.044.
29. Kazemtabrizi, B. Mathematical Modelling of Multi-terminal VSC-HVDC links in Power Systems using Optimal Power Flows. Ph.D. Thesis, Department of Electronics and Electrical Engineering, University of Glasgow, Glasgow, UK, 2011.
30. Acha, E.; Kazemtabrizi, B.; Castro, L.M. A New VSC-HVDC Model for Power Flows Using the Newton-Raphson Method. *IEEE Trans. Power Syst.* **2013**, *28*, 2602–2612, doi:10.1109/TPWRS.2012.2236109.
31. Acha, E.; Castro, L.M. A generalized frame of reference for the incorporation of multi-terminal VSC-HVDC systems in power flow solutions. *Electr. Power Syst. Res.* **2016**, *136*, 415–424.
32. Foote, C.; Djapic, P.; Ault, G.; Mutale, J.; Strbac, G. *United Kingdom Generic Distribution System (UKGDS): Defining the Generic Networks*; Technical Report; DTI Centre for Distributed Generation and Sustainable Electrical Energy: London, UK, 2005.
33. Bisschop, J.; Roelofs, M. *AIMMS Language Reference*, version 3.12; AIMMS B.V.: Haarlem, The Netherlands, 2011.
34. Giannelos, S.; Konstantelos, I.; Strbac, G. Option value of Soft Open Points in distribution networks. In Proceedings of the 2015 IEEE Eindhoven PowerTech, Eindhoven, The Netherlands, 29 June–2 July 2015; pp. 1–6, doi:10.1109/PTC.2015.7232529.